

# Competition and Cooperation of Assembly Sequences in Recurrent Neural Networks

Tristan M. Stöber<sup>1,2,3,✉</sup>, Andrew B. Lehr<sup>2,4</sup>, Marianne Fyhn<sup>2,5</sup>, and Arvind Kumar<sup>6</sup>

<sup>1</sup>Institute for Neural Computation, Ruhr University Bochum, Germany

<sup>2</sup>Centre for Integrative Neuroplasticity, University of Oslo, Norway

<sup>3</sup>Department of Neurology, University Hospital Frankfurt, Frankfurt, Germany

<sup>4</sup>Department of Neuro- and Sensory Physiology, University Medical Center Göttingen, Germany

<sup>5</sup>Department of Biosciences, University of Oslo, Norway

<sup>6</sup>Department of Computational Science and Technology, KTH Royal Institute of Technology, Stockholm, Sweden

<sup>✉</sup>Correspondence: tristan.stoeber@posteo.net

November 3, 2023

## 1 Abstract

Neural activity sequences are ubiquitous in the brain and play pivotal roles in functions such as long-term memory formation and motor control. While conditions for storing and reactivating individual sequences have been thoroughly characterized, it remains unclear how multiple sequences may interact when activated simultaneously in recurrent neural networks. This question is especially relevant for weak sequences, comprised of fewer neurons, competing against strong sequences. Using a non-linear rate model with discrete, pre-configured assemblies, we demonstrate that weak sequences can compensate for their competitive disadvantage either by increasing excitatory connections between subsequent assemblies or by cooperating with other co-active sequences. Further, our model suggests that such cooperation can negatively affect sequence speed unless subsequently active assemblies

23 are paired. Our analysis, validated by an analytically tractable linear approximation, characterizes the conditions  
24 for successful sequence progression in isolated, competing, and cooperating sequences, and identifies the distinct  
25 contributions of recurrent and feed-forward projections. This proof-of-principle study shows how even disadvan-  
26 taged sequences can be prioritized for reactivation, a process which has recently been implicated in hippocampal  
27 memory processing.

## 28 **2 Introduction**

29 Sequences of neural activity are a universal phenomenon in the brain, fundamentally underpinning a range of  
30 functions including olfactory processing (Friedrich and Laurent, 2001), birdsong generation (Hahnloser et al.,  
31 2002), motor control (Eichenlaub et al., 2020), and episodic memory encoding in the hippocampus (O’Keefe,  
32 1976; Dragoi and Buzsáki, 2006; Foster and Wilson, 2006; Diba and Buzsáki, 2007). These sequences unfold  
33 over various timescales and can be driven by either external stimuli or intrinsic mechanisms. Thus, to understand  
34 information processing in the brain, we need to comprehend the dynamics of neural activity sequences.

35 The emergence and reliable propagation of individual neural activity sequences have been extensively studied  
36 using computational models (Amari, 1977; Arnoldi and Brauer, 1996; Hertz, 1997; Diesmann et al., 1999; Abeles  
37 et al., 2004; Kumar et al., 2008; York and van Rossum, 2009; Fiete et al., 2010; Itskov et al., 2011; Lu et al.,  
38 2011; Azizi et al., 2013; Kappel et al., 2014; Chenkov et al., 2017; Murray et al., 2017; Seeholzer et al., 2019;  
39 Spreizer et al., 2019; Michaelis et al., 2020; Maes et al., 2020b,a; Spalla et al., 2021; Lehr et al., 2023). A number  
40 of studies characterized conditions for storing and reactivating multiple sequences in recurrent networks(Arnoldi  
41 and Brauer, 1996; Abeles et al., 2004; Kumar et al., 2008; Azizi et al., 2013; Maes et al., 2020a; Spalla et al.,  
42 2021; Lehr et al., 2023). However, interactions between sequences within a network are less understood, and in  
43 particular the influence of competition and cooperation on sequence reactivation has not yet come into focus.

44 A popular experimental paradigm to expose the functional role of neural activity sequences is to record the  
45 activity of hippocampal neurons in a spatial navigation task, commonly performed in rats or mice. While traversing  
46 an environment, place cells are activated in a sequential manner (O’Keefe, 1976; Dragoi and Buzsáki, 2006).  
47 Subsequently, when the animal is resting, planning or consuming, the same neural activity sequences may be  
48 reactivated (or replayed) at a faster time scale during sharp wave ripple (SPWR) events (Wilson et al., 1994;  
49 Skaggs and McNaughton, 1996; Ji and Wilson, 2007; Diba and Buzsáki, 2007). Such offline reactivation can  
50 represent multiple distinct experiences (Silva et al., 2015). However, it is assumed that normally only one sequence  
51 is reactivated per sharp-wave ripple (He et al., 2020).

52 Replay of sequences is crucial for memory consolidation (Girardeau et al., 2009; Dupret et al., 2010; Fernández-  
53 Ruiz et al., 2019; Oliva et al., 2020). Successful generation of long sequences during SWR is associated with better  
54 memory (Fernández-Ruiz et al., 2019). Moreover, the probability that a particular sequence will be reactivated  
55 varies with experience, with novel and reward-related sequences being prioritized (McNamara et al., 2014; Igata  
56 et al., 2021; Singer and Frank, 2009; Ambrose et al., 2016, but see Gupta et al., 2010). Intriguingly, the fact  
57 that neither the generation of sharp-wave ripples (Bragin et al., 1995; Yamamoto and Tonegawa, 2017) nor the  
58 reactivation of sequences (Chenani et al., 2019) are abolished by lesions or inhibition of the medial entorhinal cor-  
59 tex, the primary input structure to the hippocampus, suggests the existence of inherent mechanisms for sequence  
60 prioritization within the hippocampus.

61 Hippocampal activity sequences differ in key properties depending on which information they represent. When  
62 encoding the location of objects and other animals fewer hippocampal place cells are recruited and their firing  
63 rates are lower compared to place cells for the animal's own location (Danjo et al., 2018; Omer et al., 2018).  
64 Thus, hippocampal sequences are likely composed of differently sized cell assemblies. In the following we call  
65 sequences with large assemblies strong and those with small assemblies weak. To consolidate their corresponding  
66 experiences, it is conceivable that both weak and strong sequences compete for reactivation during SPWRs.

67 A computational model suggests that successful reactivation becomes more difficult for weak sequences,  
68 unless recurrent connections within and/or feed-forward projections between cell assemblies are strengthened  
69 (Chenkov et al., 2017). However, the required amount of potentiation increases non-linearly with decreasing  
70 assembly size, and synapses may quickly reach their physiological boundaries (Chenkov et al., 2017). If multi-  
71 ple sequences are activated at the same time, mutual inhibition between them may create a winner-take-all type  
72 competition. In such a scenario, weak sequences essentially stand no chance of winning the competition.

73 Here, we explore how weak sequences may cooperate to win over stronger sequences during replay events.  
74 Inspired by recent findings about gated synaptic plasticity and mutual feed-forward inhibition between region CA3  
75 and CA2 in the hippocampus, we proposed that co-occurring sequences in these regions may be selectively paired  
76 by the release of neuromodulatory substances (Stöber et al., 2020). In addition to linking distinct information  
77 (Mankin et al., 2015; Lee et al., 2015; Wintzer et al., 2014) in each region, mutual excitatory support between  
78 CA3 and CA2 sequences may ensure their reactivation, while at the same time recruiting sufficient inhibition to  
79 suppress competing sequences (He et al., 2020; Lehr et al., 2021).

80 To develop a theoretical understanding based on these hippocampal insights, we demonstrate that cooperation  
81 and competition of assembly sequences can be implemented in a rate-based model. Within a sequence, reliable  
82 and fast signal transmission is achieved by excitatory feed-forward projections between subsequent assemblies,  
83 employing balanced amplification (Murphy and Miller, 2009; Chenkov et al., 2017). Competition and coopera-

84 tion are implemented by feed-forward inhibition and excitation across assemblies. Characterizing conditions for  
85 competition and cooperation, we show that a) feed-forward excitation is crucial, but must remain within a certain  
86 range to avoid excessive and persistent activation, b) recurrence within assemblies helps the surviving sequence to  
87 recover, c) feed-forward inhibition can mediate competition, d) excitatory coupling between co-active assemblies  
88 allows weak sequences to win, but slows sequence progression, and e) preferentially pairing subsequently instead  
89 of co-active assemblies maintains sequence speed. Taken together, these results demonstrate that reactivation  
90 dynamics of neural sequences are shaped both by modifying feed-forward properties as well as by interactions  
91 among multiple sequences.

## 92 **3 Results**

### 93 **3.1 Conditions for progression of a single sequence**

94 We used a rate-based model with a non-linear activation function to first study the progression of a single assembly  
95 sequence (Fig. 1a,b). Each assembly is composed of discrete and recurrently interacting populations of excitatory  
96 and inhibitory neurons. Sequences are defined by connecting subsequent excitatory populations with feed-forward  
97 projections. In addition, all assemblies – independent of their position in the sequence – send feed-forward inhi-  
98 bition to each other; they send excitatory projections to each other's inhibitory populations. To start the sequence  
99 the excitatory population of the first assembly receives external stimulation. To characterize successful sequence  
100 progression, we defined four conditions: 1) All active: Within each assembly, the excitatory population must be  
101 activated at least at one point in time. 2) All informative: In addition, each excitatory population must exceed  
102 the activity of others at least one point in time. 3) Sparse activity: Global activity of the whole network must be  
103 sparse, e.g. peak activity is not to be reached by more than two assemblies at any point in time. 4) Order: Peak  
104 activation of any excitatory population must maintain its predefined order.

105 Successful sequence progression depends on both recurrent and feed-forward projections. The strength of  
106 each connection is a product of the respective excitatory or inhibitory population size,  $M^{\{E,I\}}$ , synaptic strength,  
107  $g^{\{E,I\}}$  and recurrent or feed-forward connection probability,  $p_{\{rc,ff\}}$ . To investigate the dependence of sequence  
108 progression on connection strength, we systematically varied  $p_{rc}$  and  $p_{ff}$ , simultaneously for excitatory and  
109 inhibitory projections. We found that the parameter region allowing successful sequence progression for  $p_{ff}$  is  
110 relatively narrow compared to  $p_{rc}$  (Fig. 1c, black region). Closer investigation revealed that, without sufficient  
111 feed-forward projections, activity dies out ( $s^1$  in Fig. 1d), preventing all assemblies from being activated (Fig.  
112 1f), violating condition 1 (Fig. 1g). By contrast, strong feed-forward projections led to rapid and persistent

113 activation ( $s^4$  in Fig. 1d, 1e), violating the condition 2 (Fig. 1h). However, if excitatory and inhibitory populations  
114 recurrently interact with sufficient strength, assembly activation can become transient, allowing sequences to  
115 progress in a sparse fashion for an increasing range of feed-forward weights, condition 3 ( $s^2$  and  $s^3$  in Fig. 1d).

116 The V-shape of the parameter region reflecting successful progression illustrates the dual role of recurrent  
117 interactions. On its left flank (for weak feed-forward connections), increasing recurrent interactions,  $p_{rc} > 0.025$ ,  
118 decreases the required feed-forward weights,  $p_{ff}$  by positively amplifying weak inputs. On the right flank (for  
119 strong feed-forward connections), stronger recurrent inhibition prevents persistent activity and, thus, increases  
120 permissible feed-forward weights.

121 Progression of single assembly sequences can be approximated by an even simpler linear dynamical system  
122 (Chenkov et al., 2017). Under the assumption of stationarity, we analytically determined the minimal value of  $p_{rc}$   
123 required for sustained activity in subsequent assemblies in relation to  $p_{ff}$  (for details see Methods). We show the  
124 simulation results are in close agreement to the analytically determined values of  $p_{rc}$  and  $p_{ff}$  for  $p_{rc} > 0.025$  (Fig.  
125 1c, red line). For  $p_{rc} < 0.025$  the analytical approximation diverges from the simulation results (see Discussion).  
126 For very low recurrence values,  $p_{rc} \sim 0$ , sequence progression is limited to few specific values of  $p_{ff}$  ( $s^0$  in Fig.  
127 1d, 1e). Note that the solutions of the the linear approximation are influenced by a scaling factor  $c$ , related to the  
128 slope of the neuron's input-output function. Throughout the article, we retain  $c = 0.163$ , as determined by solving  
129 for  $c$  under the parameters of example sequence  $s^2$  (see Methods).

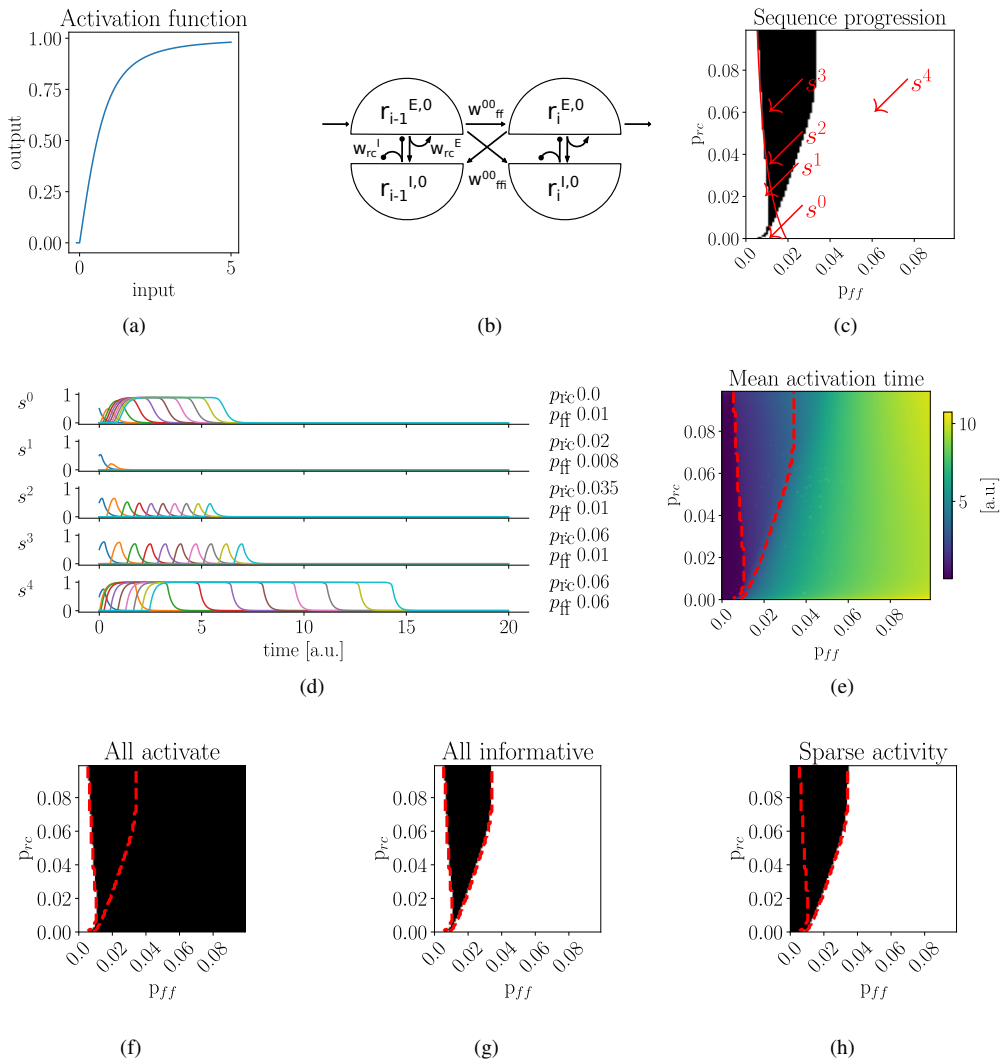


**Figure 1: Recurrent and feed-forward interactions influence the progression of a single sequence.** **a)** Non-linear activation function of excitatory and inhibitory populations. **b)** Connections within and between assemblies in a single sequence. Each assembly is formed by two recurrently interacting populations, representing excitatory ( $E$ ) and inhibitory ( $I$ ) neurons. A given sequence  $s^0$  is established by connecting subsequent excitatory populations via feed-forward excitatory projections with strength  $w_{ff}^{00}$ . Assemblies generally suppress each other via feed-forward inhibition; excitatory projections from excitatory to all inhibitory populations of other assemblies with strength  $w_{ff}^{00_m}$ . **c)** Successful sequence progression, black region, depends on both recurrent,  $p_{rc}$  and, feed-forward,  $p_{ff}$ , connection probability. Red line, analytic solution of the linearized rate model for sustained activity propagation. For low values of  $p_{rc}$ , the non-linear rate model and the analytic solution diverge. **d)** Example sequences, corresponding to red arrows in b). Only  $s^2$  and  $s^3$  successfully reactivate. Activity  $r_i^{E,j}$  of every third excitatory population is shown. Different colors correspond to different excitatory populations. **e)** Mean activation time across all assemblies. Large values of  $p_{ff}$  lead to persistent activity and, thus, to large mean activation time. **f)** Parameter region (black) where all excitatory populations in sequence become activated, fulfilling condition 1: *All active*. **g)** Parameter region fulfilling condition 2: *All informative*, all excitatory populations must exceed activity of others at least once (black). **h)** Parameter region fulfilling condition 3: *Sparse activity*. Red, dashed contours in c), e), f) and g) correspond to black region for successful sequence progression in b).

### 130 3.2 Competition between two sequences

131 Next, we studied competition between two sequences,  $s^0$  and  $s^1$ . As before, each assembly sends feed-forward  
132 inhibition to all other assemblies, both within and between sequences (Fig. 2a). If the first assemblies in both  
133 sequences are simultaneously activated, the interplay between excitation within the assemblies and inhibition  
134 between sequences can lead to one of four scenarios: a) Activity in both sequences ceases before the sequence  
135 is completed; referred to as *no winner*; b)  $s^0$  successfully progresses and  $s^1$  ceases; referred to as  $s^0$  *wins*; c)  $s^1$   
136 successfully progresses and  $s^0$  ceases; referred to as  $s^1$  *wins*; d) both sequences successfully progress; referred to  
137 as *both win*.

138 To exemplify competition dynamics, we let two sequences compete for a given set of parameters (Fig. 2b).  
139 After an initial surge, activity diminished in both sequences. While  $s^1$  ceased, activity in  $s^0$ , with slightly larger  
140 assemblies, recovered and successfully progressed.

141 The competition outcome depends on assembly sizes as well as interactions within and between sequences.  
142 To systematically characterize the occurrence of the four competition scenarios, we varied assembly sizes  $M^{E,0}$ ,  
143  $M^{E,1}$  for different connection probabilities of either feed-forward excitation  $p_{ff}$ , recurrent excitation  $p_{rc}$ , or  
144 feed-forward inhibition  $p_{ffi}$ . Note, in the following, sizes of the inhibitory populations,  $M^{I,0}$ ,  $M^{I,1}$ , are scaled  
145 accordingly to maintain a constant ratio of excitatory and inhibitory population sizes.

146 For example, for moderate levels of feed-forward excitation,  $p_{ff} = 0.014$ , relatively large assemblies,  
147  $M^{E,0}, M^{E,1} > 1400$  were required for one sequence to win over the other (Fig. 2c, central row in left column).  
148 Nevertheless, even for large assemblies, the difference between sequences had to be prominent, otherwise both  
149 sequences ceased to exist. By contrast, if feed-forward excitation is increased, even moderately sized assembly  
150 sequences could win as long as they are larger than their competitor (Fig. 2c, bottom row in left column). As a  
151 consequence of this, the fraction of the  $M^{E,0}, M^{E,1}$  parameter space spanned by either  $s^0$  or  $s^1$  winning increased  
152 with a rise in the strength of feed-forward connections,  $p_{ff}$ , until it hit an upper bound (Fig. 2c, upper row in left  
153 column).

154 Without recurrence, even sequences with large assemblies failed to successfully propagate when competing.  
155 As we showed in Figure 1c and know from the literature on synfire chains (Hertz, 1997; Diesmann et al., 1999;  
156 Kumar et al., 2010), individual sequences can progress without recurrent interactions. However, we hypothesized  
157 that in a competition scenario, recurrence is paramount for the surviving sequence to recover. To test this, we  
158 characterized the competition outcome for a range of assembly sizes given different values of  $p_{rc}$ . Consistent  
159 with our expectation, for relatively weak recurrence,  $p_{rc} = 0.015$ , larger assemblies were required to avoid that  
160 both sequences cease their progression (Fig. 2c, central row in central column). Surprisingly, we found that weak

161 recurrence allows both strong sequences to win (Fig. 2c, black region, central row in central column). With an  
162 increase in the recurrence,  $p_{rc} = 0.03$ , the fraction of the  $M^{E,0}, M^{E,1}$  parameter space spanned by either  $s^0$  or  $s^1$   
163 winning increased (Fig. 2c, bottom row in central column). Thus, we conclude that recurrence is indeed crucial  
164 when sequences compete.

165 Feed-forward inhibition ensures that only one sequence wins. Here, sequences competed by inhibiting each  
166 other. Therefore, we expected that relatively weak feed-forward inhibition will allow both sequences to win. Again  
167 classifying competitions outcomes, we could indeed show that for low values of  $p_{ffi}$  a considerable fraction of  
168 the  $M^{E,0}, M^{E,1}$  parameter space was covered by the *both win* scenario (Fig. 2c, black region, upper and central  
169 row, right column). Further, we found that weak feed-forward inhibition corresponded to a large fraction of failed  
170 progressions for both sequences, *no winner*. Without inhibition between assemblies of the same sequence, activity  
171 in each cell assembly became persistent, violating the sparsity condition (data not shown). On the other hand,  
172 when  $p_{ffi}$  was increased, the *both win* case disappeared (Fig. 2c, upper and bottom row, left column).

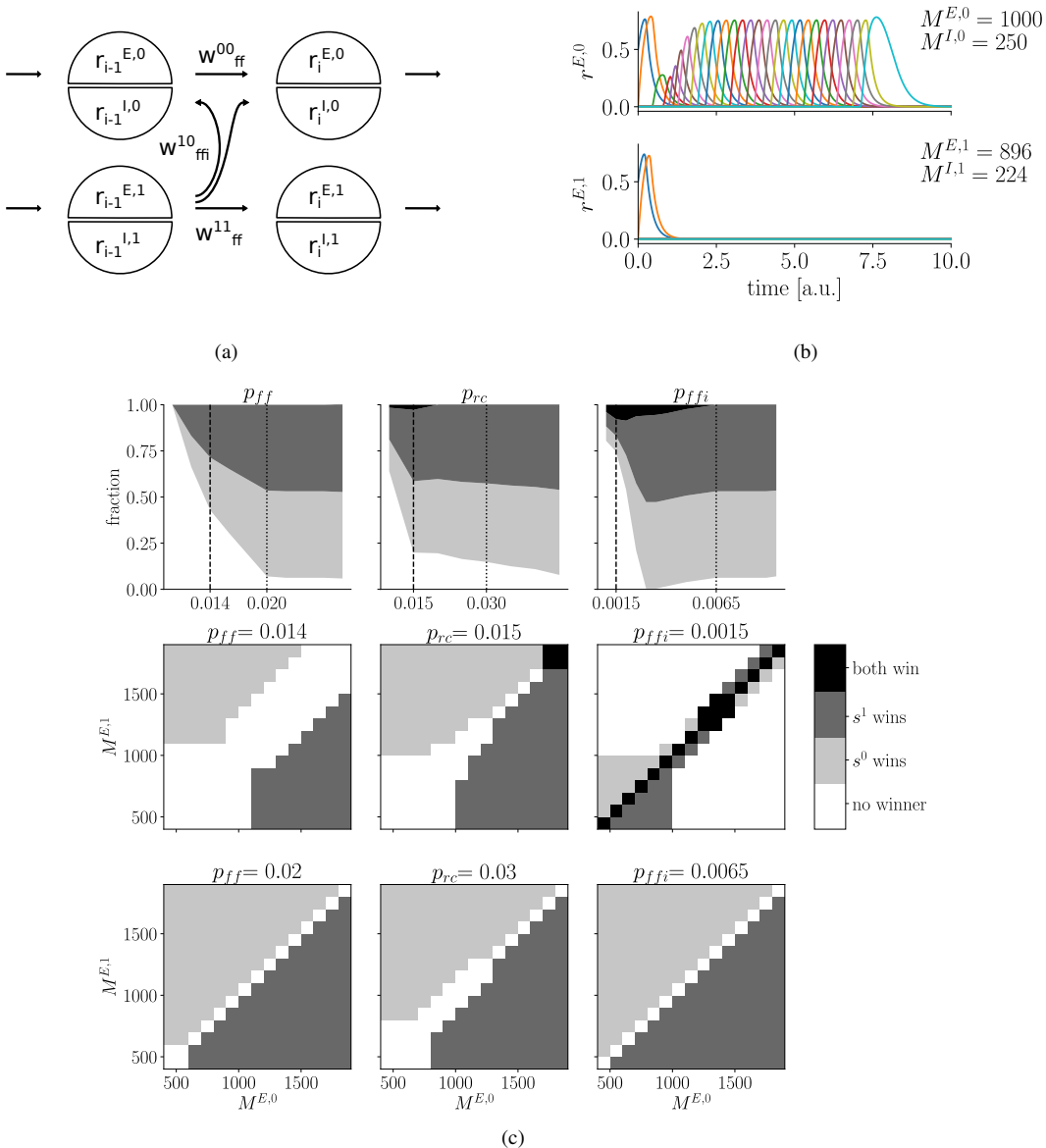


**Figure 2: Competition between two sequences.** **a)** Scheme of connections for competition scenario. Two sequences,  $s^0$  and  $s^1$ , compete via feed-forward inhibition between all assemblies. For visual clarity, only feed-forward inhibition with strength  $w_{ff}^{01}$  from one assembly of  $s^0$  to two assemblies of  $s^1$  is shown. **b)** Example: Larger sequence  $s^0$  wins over  $s^1$ . Only activities of excitatory populations are shown. Both sequences suppress each other's activity until  $s^1$  ceases and  $s^0$  recovers. Colors repeat after 10 assemblies. **c)** Competition scenarios for different values of feed-forward, recurrent, and feed-forward inhibition connection probability.  $p_{ff}$ ,  $p_{rc}$ ,  $p_{ffi}$  are separately varied. Middle and bottom rows exemplify competition outcomes when scanning the  $M^{E,0}, M^{E,1}$  space for different values of  $p_{ff}$ , left,  $p_{rc}$ , center, or  $p_{ffi}$ , right. Upper row summarizes the distribution of competition scenarios for each scan of the  $M^{E,0}, M^{E,1}$  space. Specific values of low and high value examples are indicated by dashed and pointed lines, corresponding to upper and center rows.

173 Compensating for small assemblies by increasing feed-forward weights may become physiologically implau-  
 174 sible. As proposed in (Stöber et al., 2020), a weak sequence, comprised of smaller assemblies, competing with a

175 strong sequence, can ensure progression by further potentiating feed forward weights. However, we hypothesized  
176 that the required amount of potentiation scales non-linearly with assembly size – as already shown for individ-  
177 ual sequences (Chenkov et al., 2017) – and therefore, may hit physiological boundaries for weak sequences. We  
178 explicitly tested this prediction by varying the respective parameters for sequence  $s^1$ ; keeping parameters in  $s^0$   
179 fixed. In agreement with the hypothesis, we found a non-linear increase in the required feed-forward connection  
180 probability  $p_{ff}^{11}$  for decreasing assembly sizes  $M^{E,1}$  (Fig. 3a). If both assembly sizes and feed-forward weights  
181 were strong (*no winner region* in upper right corner of Fig. 3a), persisting activity violated both the activation and  
182 the sparsity condition (data not shown).

183 To gain an analytic understanding of the competition scenario, we extended the simplified linear rate model to  
184 include a second sequence. Keeping the activation of excitatory populations in  $s^0$ , we solve for  $p_{ff}^{11}$ , the minimal  
185 required feed-forward weight to ensure sustained activity of  $s^1$  (Fig. 3a, red line, see Methods). However, the an-  
186 alytic solution predicts lower required weights compared to the rate-model simulation. One potential explanation  
187 for this difference may be that feed-forward inhibition in the rate model is between all assemblies, while it is only  
188 to the next competing assembly in the simplified linear model (see Discussion).

189 To compare the presented results to a situation without competition, we repeated the simulation and analytic  
190 calculations with silenced  $s^0$  (Fig. 3b). As before, the required feed-forward connection probability increased  
191 non-linearly with decreasing assembly size. However, without a competing sequence, also smaller feed-forward  
192 connection probabilities allowed successful propagation. This holds true for both the analytical prediction and  
193 the simulation results. In conclusion, these findings show that competition increases the required strength of  
194 feed-forward weights, making it even more difficult to reactivate sequences with small assemblies.

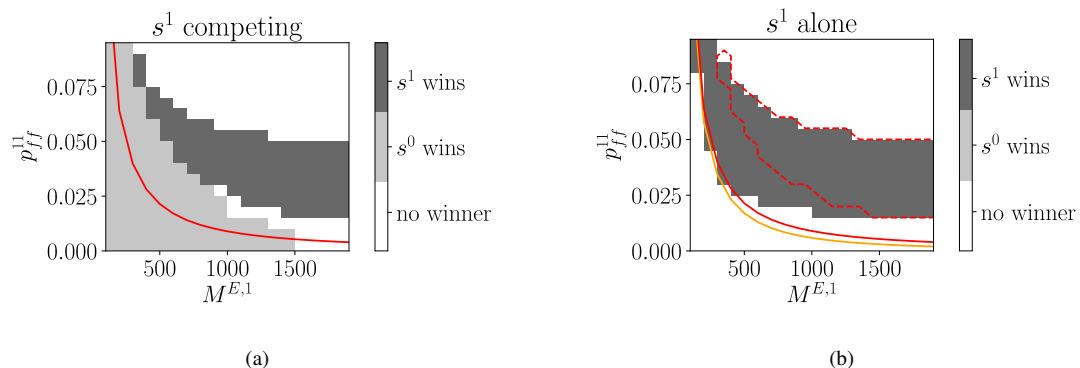


**Figure 3: Competition makes it harder for sequences with small assemblies to ensure progression by strengthening feed-forward weights.** **a)** For fixed parameters of  $s^0$ ,  $M^{E,0} = 1000$ ,  $p_{ff}^{00} = 0.02$ , assembly size  $M^{E,1}$  and feed-forward connection probability  $p_{ff}^{11}$  of  $s^1$  are varied. For  $s^1$  to win (dark area), smaller assemblies must be compensated by increasingly larger feed-forward weights. Red line, analytic prediction of linearized rate model for sustained activity propagation in  $s^1$  with constant activity in  $s^0$ ,  $r_i^{E,0} = 1$ . **b)** Same as a), but without activating  $s^0$ . Orange line, analytic prediction for sustained activity propagation in  $s^1$  with  $s^0$  silenced. Red dashed contour line reflects  $s^1$  wins area and red line analytic prediction from competition scenario in a).

### 195 3.3 Cooperation and competition between three sequences

Given the physiological limits on the potentiation of feed-forward projections, an alternative or additional way for sequences to ensure progression despite competition is to mutually support each other. This may happen if simultaneously active assemblies in co-occurring sequences are paired by Hebbian plasticity (Stöber et al., 2020). To demonstrate both cooperation and competition between assembly sequences, we created a minimal scenario with one strong, and two weak sequences (Fig. 4a). As before, all assemblies mutually inhibited each other and the excitatory populations at the start of each sequence were simultaneously activated. The strong sequence  $s^0$  has a competitive advantage due to its larger assemblies. As expected, without any cooperation between  $s^1$  and  $s^2$ , sequence  $s^0$  won (case  $c_0$ , Fig. 4b, Fig. 4c).

When weak sequences were able to cooperate, they could however overcome a strong competitor. We introduced feed-forward excitatory projections between co-active excitatory populations in  $s^1$  and  $s^2$ , summarized by their strengths  $w_{ff}^{12}$  and  $w_{ff}^{21}$ . Given sufficient mutual support,  $s^1$  and  $s^2$  were able to out-compete  $s^0$  ( $c_1$ , Fig. 4b, Fig. 4c). However, the stronger the mutual excitatory connections, the longer were the activation times of excitatory populations ( $c_1$  vs.  $c_2$ , Fig. 4d). Increasing the excitatory interactions further led to persistent activity in the first assemblies, halting successful sequence progression ( $c_3$ , Fig. 4c, 4e, 4f).

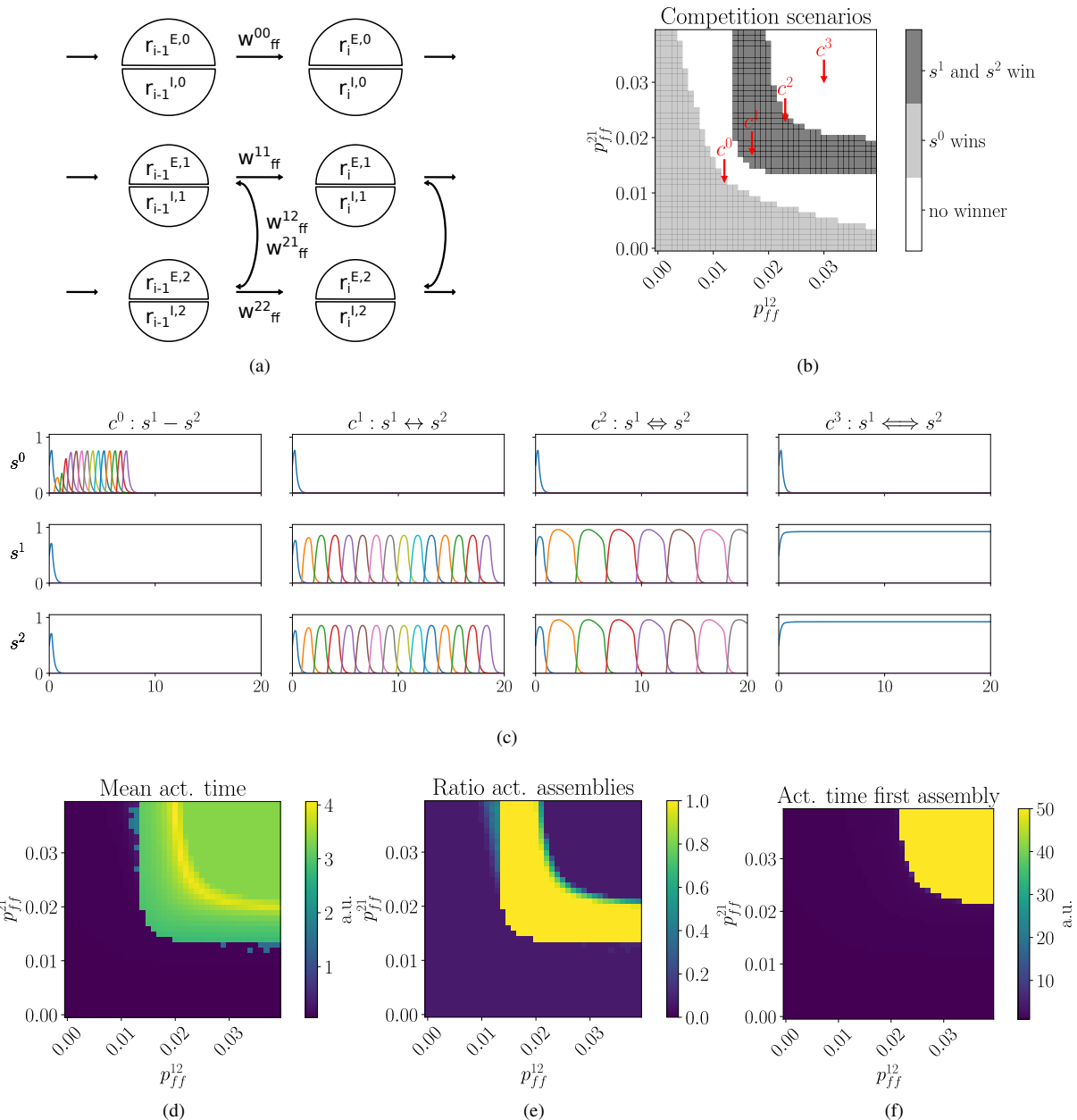


**Figure 4: Cooperation via mutual excitation between assembly sequences.** **a)** Network scheme for competition and cooperation between discrete assembly sequences. Sequence with larger assemblies,  $s^0$ , competes with  $s^1$  and  $s^2$ . Competition via feed-forward inhibition between all sequences not shown. Cooperation between  $s^1$  and  $s^2$  through reciprocal excitatory connections to co-active assemblies with strength  $w_{ff}^{12}$  and  $w_{ff}^{21}$ . Larger assemblies of  $s^0$  are indicated by larger circles. **b)** Connection probabilities between  $s^1$  and  $s^2$ ,  $p_{ff}^{12}$  and  $p_{ff}^{21}$ , are varied. Sufficiently strong mutual excitation is required for  $s^1$  and  $s^2$  to outcompete  $s^0$ . **c)** Examples:  $c_0 : s^1 - s^2$ , mutual excitatory interactions between  $s^1$  and  $s^2$  not sufficient;  $c_1 : s^1 \leftrightarrow s^2$ , pairing between  $s^1$  and  $s^2$  strong enough to win;  $c_2 : s^1 \Leftrightarrow s^2$ , increased excitatory interactions lead to slower sequence progression, e.g. longer activation times;  $c_3 : s^1 \Leftrightarrow s^2$ , if excitatory interactions are too strong, sequence progression fails because first assemblies of  $s^1$  and  $s^2$  remain active. Only activity of excitatory populations is shown. **d)** Mean activation times of excitatory populations in  $s^1$ . Strong mutual excitation leads to longer activation times and slow sequence progression. **e)** Ratio of activated excitatory populations in  $s^1$ . Only in region with successful cooperation with  $s^2$  all assemblies of  $s^1$  are activated. **f)** Activation time of first excitatory population in  $s^1$ . Strong interactions halt propagation, because early assemblies maintain activity over the full simulation duration.

210 **3.4 Potentiation of excitatory synapses to subsequently active assemblies in paired se-**  
211 **quence increases propagation speed**

212 In the previous section we observed that pairing sequences by potentiating co-active assemblies can indeed facil-  
213 itate their reactivation, but it slows sequence progression and, if too strong, leads to persistent activity. Thus, we  
214 hypothesized that sequence speed can be increased by introducing excitatory projections to subsequently active  
215 assemblies (see Fig. 5a). Adding this type of projection to the three sequence model and explicitly measuring  
216 sequence speed by the inverse of the median interpeak interval of excitatory populations, we observed a range of  
217 different speeds depending on the relative levels of potentiation between co-active and subsequent assemblies (Fig.  
218 5b,5c). As expected, stronger potentiation between co-active assemblies led to slower progression (purple region,  
219 Fig. 5b). Additionally increasing the synaptic strength between subsequent while maintaining strong synapses be-  
220 tween co-active assemblies marginally increased speed at the expense of prolonged activation times of individual  
221 assemblies ( $c^0$  vs.  $d^0$  and  $d^1$ ). However, reducing synapse strength between co-active while maintaining relatively  
222 strong synapses to subsequent assemblies can increase sequence speed up to the level of the competing sequence  
223  $s^0$  (yellow region, Fig. 5b; example  $d^2$ , Fig. 5c). Thus, potentiating subsequently active assemblies can indeed  
224 facilitate reactivation of paired sequences while preserving the timescale of sequence progression.

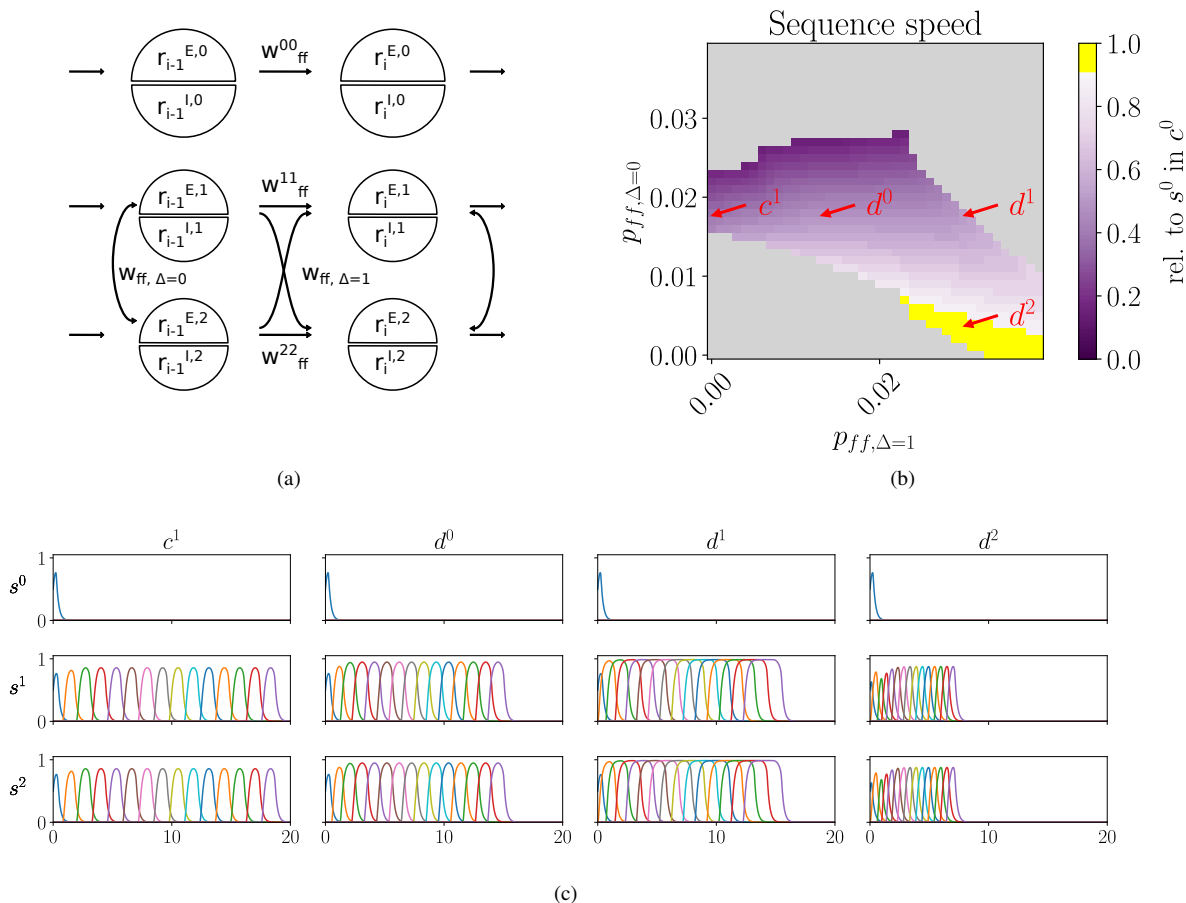


**Figure 5: Shifting feedforward excitation from co-active to subsequent assemblies increases speed of co-operating sequences.** **a)** Beyond prior simulations which modified feedforward excitation solely between simultaneously active assemblies,  $w_{ff, \Delta=0}$ , we also introduce feedforward excitation to subsequent assemblies,  $w_{ff, \Delta=1}$ , in cooperating sequences  $s^1$  and  $s^2$ . **b)** Sequence speed of  $s^1$ , relative to  $s^0$  of scenario  $c^0$  from Fig. 4b. Successful reactivations of  $s^1$  and  $s^2$  are shown for reduced (shades of purple) and similar speed as competing sequence (yellow interval, from 0.9-1.). Non-successful reactivations are indicated in grey. Adjustments in weights  $w_{ff, \Delta=0}$  and  $w_{ff, \Delta=1}$  are achieved by altering the corresponding connection probabilities  $p_{ff, \Delta=0}$  and  $p_{ff, \Delta=1}$ . **c)** Examples:  $c^1$  - From Fig. 4b without pairing between subsequently active assemblies  $d^0$  - Increasing feedforward excitation to subsequent assemblies can counterbalance the reduced speed brought on by the additional feedforward excitation between co-active assemblies.  $d^1$  - Further increasing feedforward excitation to subsequent assemblies expands activation duration of individual assemblies.  $d^2$  - To reach speed of competing sequence  $s^0$  from scenario  $c^0$ , feedforward excitation to co-active assemblies must be reduced.

## 225 4 Discussion

226 Using a non-linear rate-based model with discrete and pre-configured assemblies, we provided a proof-of-principle  
 227 for competition and cooperation between neural activity sequences. The model allowed us to study the dynamics  
 228 of isolated, competing and cooperating sequences. Characterizing conditions for successful sequence progression,

229 we can attribute specific roles to the interactions within and between assemblies. Projections between subsequent  
230 excitatory populations ensure sequence progression. However, if too weak, activity does not propagate, and if  
231 too strong, activity saturates. Recurrent excitatory and inhibitory interactions implement balanced amplification  
232 which boosts weak excitatory inputs and prevents saturating activity (Murphy and Miller, 2009; Hennequin et al.,  
233 2012). Thus, with increasing recurrency, a larger range of excitatory inputs is permissible. Further, the boost  
234 of weak inputs is especially beneficial in the competition scenario and allows the surviving sequence to quickly  
235 recover. Excitatory interactions between co-active assemblies allow weak sequences to win against a stronger  
236 competitor, but such interactions slow the propagation of activity. Shifting feedforward excitation from co-active  
237 to subsequent assemblies of cooperating sequences increases sequence speed, enabling successful replay without  
238 slowing sequence propagation.

239 In the case of a single sequence, the analytically predicted minimal feed-forward and recurrent weights are in  
240 close agreement to the non-linear rate model. We contrasted the simulation results with an even simpler model of  
241 assembly sequence progression, comprised of a linear dynamical system and with only projections to subsequent  
242 assemblies (Chenkov et al., 2017). Assuming that the activation time of a preceding excitatory population is much  
243 longer than the rise time of the subsequent excitatory population, we derived conditions for sustained activity  
244 propagation. For moderate and large recurrent connection strengths, the simulation quantitatively agreed with  
245 the analytic prediction. As part of the analytic approximation, we used the same scaling factor as Chenkov et al.  
246 (2017). This factor has been fitted to match the lower bounds for sequence progression in a spiking neural network.  
247 Thus, the estimated conditions for successful progression should translate to similar dynamics in a spiking neural  
248 network.

249 For weak recurrent interactions, the results of the non-linear network deviate from both the analytic approxi-  
250 mation and a previously published spiking neural network (Fig. 1c, Chenkov et al., 2017). Even without recurrent  
251 interactions, the non-linear rate model allows single sequence progression for a very narrow range of feed-forward  
252 projections. However, in contrast to the analytical approximation and the spiking model, weaker feed-forward  
253 interactions are required in the non-linear rate model. A definite explanation requires further investigation. Poten-  
254 tially, the divergence is a result of the different wiring of feed-forward inhibition. In the non-linear rate model, all  
255 assemblies, even when in the same sequence, send and receive feed-forward inhibition. In the analytic approxi-  
256 mation there is no feed-forward inhibition within a sequence, only between sequences. In the published spiking  
257 model feed-forward inhibition is not assembly specific and connection strengths are plastic, making it difficult to  
258 compare (Chenkov et al., 2017).

259 Our results highlight a key constraint on which synapses may be potentiated to support successful pairing of  
260 activity sequences. We report that direct excitatory interactions between co-active assemblies lead to increased

activation times (Fig. 4) and slower sequence propagation (Fig. 5). Maintaining propagation speed for paired sequences was made possible by potentiating excitatory projections to subsequently active excitatory populations in the cooperating sequence. Such temporally skewed potentiation may naturally occur via asymmetric spike-timing-dependent plasticity during encoding (Klos et al., 2018; Miner and Tetzlaff, 2020). We note that several other mechanisms may modulate speed: Dynamic firing rate adaptation to mimic refractory periods (Wilson and Cowan, 1972), inhibitory oscillations to rhythmically gate propagation (Recanatesi et al., 2015), or inhibitory plasticity to maintain EI balance (Vogels et al., 2011).

The presented results equally relate to the creation of new synapses as well as to potentiation of existing synapses. The strength of an individual connection is defined by the product of population size, the average connection probability and the synaptic weight. Unlike population size which also affects other projections of this population, the specific connection probability and synaptic weight are interchangeable scaling factors.

Weak sequences may also compensate for small assembly sizes by potentiating recurrent interactions, weakening feed-forward inhibition, or recruiting more neurons (assembly outgrowth, see Tetzlaff et al., 2015; Lehr et al., 2022). Here, the underlying learning scenario is highly simplified. We assume that during learning pre-configured, recurrently interacting assemblies are activated by external input. This is thought to induce the formation or potentiation of excitatory projections between subsequently activated excitatory populations. For this reason we only evaluated the possibility that weak sequences compensate for small assemblies by strengthening projections between subsequent excitatory populations.

Competition between neural activity sequences may be directly observed in hippocampal recordings. If reactivation of neural activity sequences in the hippocampus is indeed the outcome of a competition process, signatures of this process should be detectable. In the presented model, competition dynamics are characterized by an initial rise in the activity of assemblies of different sequences, followed by reduced activity due to mutual inhibition, until one sequence starts to out-compete the others. Such dynamics should be particularly strong if competing sequences are of equal strength. Studying the reactivation of place cell sequences after running on two or more distinct linear tracks may be an adequate experimental paradigm (Silva et al., 2015; He et al., 2020).

In summary, our work investigated the interaction of multiple sequences of different strengths within a recurrently connected network. We considered scenarios of competition and cooperation between interacting sequences and characterized the effects on sequence reactivation and sequence dynamics. We showed that pairing weak sequences allows them to win over a stronger competitor. This has implications for hippocampal replay – the number of hippocampal neurons recruited to represent certain types of information strongly differ between sensory modalities (Salz et al., 2016; Danjo et al., 2018), thus making it important to develop a theoretical understanding of how heterogeneity in assembly size influences replay statistics.

## 293 5 Methods

294 Simulations and analysis were performed with Jupyter notebooks 6.0.3 and Python 3.7.8 with standard libraries,  
 295 such as NumPy 1.18.5, SciPy 1.18.5, Matplotlib 3.2.2 and SymPy 1.5.1. All code is available at [https://github.com/tristanstoeber/sequence\\_competition\\_cooperation](https://github.com/tristanstoeber/sequence_competition_cooperation).

### 297 5.1 Assembly sequences in a non-linear rate model

In the non-linear rate model each assembly is formed by one excitatory and one inhibitory population. The evolution of rate,  $r_i^j$ , of a given population  $i$  of sequence  $s^j$  is described by

$$\tau \frac{dr_i^j}{dt} = -r_i^j + S(x) \quad (1)$$

298 with  $\tau$  a fixed population time constant, equal across all populations.

The sigmoidal activation function  $S$  over the input  $x$  is defined by

$$S(x) = H\left(\frac{(x-a)}{\sqrt{(x-a)^2+1}}\right) \quad (2)$$

299 with the Heaviside function  $H$  (compare Fig. 1a) and  $a = 1 \times 10^{-7}$  a small constant rightward shift of the  
 300 activation function, preventing numerical imprecision around  $x = 0$  from inadvertently driving network activity.

Each population in sequence  $s^j$  receives input by recurrent excitatory and inhibitory projections with strengths  $w_{rc}^{E,j}$  and  $w_{rc}^{I,j}$ . Excitatory populations may receive additional excitatory input by the preceding assembly of the same sequence with strength  $w_{ff}^{jj}$ . In the case of cooperating sequences, each excitatory population receives excitatory input of a co-active assembly of another sequence  $s^m$  with strength  $w_{ff}^{mj}$ . All assemblies send feed-forward inhibition to each other, e.g. they excite each others inhibitory population. Thus, in addition to the recurrent input  $w_{rc}^{E,j}$  from their associated excitatory population, they receive input  $w_{ffi}^{mj}$  from all remaining  $n$  excitatory populations  $r_n^{E,m}$  of all sequences  $s^m$ . Thus, the full input to an excitatory population  $x_i^{E,j}$  and an inhibitory population  $x_i^{I,j}$  of assembly  $i$  in sequence  $s^j$  is described by:

$$x_i^{E,j} = w_{rc}^{E,j} r_i^{E,j} + w_{rc}^{I,j} r_i^{I,j} + w_{ff}^{jj} r_{i-1}^{E,j} + w_{ff}^{mj} r_n^{E,m} \quad (3)$$

$$x_i^{I,j} = w_{rc}^{E,j} r_i^{E,j} + w_{rc}^{I,j} r_i^{I,j} + \sum_m \sum_{n \neq i} w_{ffi}^{mj} r_n^{E,m} \quad (4)$$

301 Weight values are the product of the number of excitatory,  $M^{E,j}$ , and inhibitory,  $M^{I,j}$ , neurons in the sending  
302 population, equal for all assemblies in a given sequence  $s^j$ , as well as recurrent,  $p_{rc}$ , feed-forward,  $p_{ff}$ , and  
303 feed-forward inhibitory,  $p_{ffi}$ , connection probabilities and excitatory,  $g^E$ , or inhibitory,  $g^I$ , synaptic strengths.

$$w_{rc}^{E,j} = M^{E,j} p_{rc} g^E \quad (5)$$

$$w_{rc}^{I,j} = M^{I,j} p_{rc} g^I$$

$$w_{ff}^{mj} = M^{E,m} p_{ff} g^E$$

$$w_{ffi}^{mj} = M^{E,m} p_{ffi} g^E$$

304 Sequences are comprised of  $n_{ass}$  assemblies, all assemblies within a given sequence are equal in size and the  $E/I$   
305 size ratio is fixed to  $M^E/M^I = 4$ .

## 306 5.2 Simulation and data analysis

307 Simulations were run for a fixed time interval and a fixed step size with the solve\_ivp function in SciPy's integrate  
308 package with integration method LSODA. As initial condition, the excitatory population in the first assembly of  
309 each activated sequence  $s^j$  is set to  $r_0^{E,j} = 0.5$ , while all other rates are at zero.

310 To be classified as successfully progressing, a sequence must satisfy the following four conditions: 1) All  
311 active: All assemblies must be activated. There should exist at least one point in time during which the activity of  
312 a given excitatory population exceeds a minimal threshold  $r_{min}$ . 2) All informative: Each excitatory population  
313 must exceed the activity of others at least one point in time. 2) Sparse activity: While the sequence is running,  
314 maximum firing rates at any given point in time must not be reached by more than two assemblies. To exclude  
315 numerical edge cases we consider assemblies to have similar firing rates, whenever the absolute value of the  
316 difference is less than  $r_{tol}$ . Allowing two assemblies to both have peak activity is necessary for the time points  
317 when decreasing activity of the previous and increasing activity of the subsequent assembly are equal. 4) Order:  
318 Activation times must maintain sequence order. The order of peak activities agrees with the predefined order of  
319 assemblies in the sequence. Given our predefined one-step feed-forward interactions this is almost always the  
320 case, though we mention it for completeness.

321 Sequence speed is determined as the inverse of the median interpeak interval of excitatory populations. Before  
322 determine timepoints of peak activation, we rounded values to a precision of  $r_{tol}$  and ignored values below  $r_{min}$   
323 to avoid numerical fluctuations to be considered a.

<sup>324</sup> For a summarized description of all parameters used in the non-linear rate model see Table 1. For a summary  
<sup>325</sup> of all used parameters see Table 2.

### <sup>326</sup> 5.3 Linearized approximation of assembly sequence progression

We approximate assembly sequence progression in a linear dynamical system, as in Chenkov et al. (2017). To study both sequence competition and cooperation, we define three sequences:  $s^0, s^1, s^2$ . Each assembly in position  $i$  of sequence  $s^j$  is described by the rate of its excitatory  $r_i^{E,j}$  and inhibitory  $r_i^{I,j}$  population. We combine population rates in a single vector  $r_i = (r_i^{E,0}, r_i^{I,0}, r_i^{E,1}, r_i^{I,1}, r_i^{E,2}, r_i^{I,2})^T$  and write the full system as

$$\tau \frac{dr}{dt} = (-\mathbb{1} + M_{rc})r_i + M_{ff}r_{i-1} \quad (6)$$

with the unity matrix  $-\mathbb{1}$  representing self-dampening,  $M_{rc}$  recurrent interactions and  $M_{ff}$  feed-forward projections from preceding assemblies to the same or other sequences. In each assembly excitatory and inhibitory populations are recurrently interacting (see Fig. 1b). Excitatory recurrent projections between assemblies of sequence  $s^j$  are summarized by  $w_{rc}^j$ , representing the number of participating neurons, connection probabilities and connection weights. Recurrent inhibitory projections,  $-kw_{rc}^j$ , are scaled by factor  $k$ , the relative strength of inhibition, summarizing both differences in inhibitory populations sizes and synaptic weights. Thus all recurrent interactions are represented by:

$$M_{rc} = \begin{pmatrix} w_{rc}^0 - 1 & -kw_{rc}^0 & 0 & 0 & 0 & 0 \\ w_{rc}^0 & -kw_{rc}^0 - 1 & 0 & 0 & 0 & 0 \\ 0 & 0 & w_{rc}^1 - 1 & -kw_{rc}^1 & 0 & 0 \\ 0 & 0 & w_{rc}^1 & -kw_{rc}^1 - 1 & 0 & 0 \\ 0 & 0 & 0 & 0 & w_{rc}^2 - 1 & -kw_{rc}^2 \\ 0 & 0 & 0 & 0 & w_{rc}^2 & -kw_{rc}^2 - 1 \end{pmatrix} \quad (7)$$

<sup>327</sup>

To simplify the mathematical treatment, we model interactions of assemblies within and between sequences only via excitatory feed-forward projections to subsequently active assemblies (Fig. 1b). As such, feed forward projections from sequence  $s^j$  to  $s^m$  originate from excitatory populations and target either the excitatory or the

inhibitory population with strength  $w_{ff}^{jm}$  and  $w_{ffi}^{jm}$ , respectively.

$$M_{ff} = \begin{pmatrix} w_{ff}^{00} & 0 & w_{ff}^{10} & 0 & w_{ff}^{20} & 0 \\ 0 & 0 & w_{ffi}^{10} & 0 & w_{ffi}^{20} & 0 \\ w_{ff}^{01} & 0 & w_{ff}^{11} & 0 & w_{ff}^{21} & 0 \\ w_{ffi}^{01} & 0 & 0 & 0 & w_{ffi}^{21} & 0 \\ w_{ff}^{02} & 0 & w_{ff}^{12} & 0 & w_{ff}^{22} & 0 \\ w_{ffi}^{02} & 0 & w_{ffi}^{12} & 0 & 0 & 0 \end{pmatrix} \quad (8)$$

328 Under the assumption that the activity in the previous assembly persists much longer than the population time  
 329 constant  $\tau$ , we can consider the steady state  $\tau \frac{dr}{dt} = 0$  as a sufficient approximation. With this, we can further  
 330 simplify the system to:

$$\begin{aligned} \vec{0} &= (-\mathbb{1} + M_{rc})r_i + M_{ff}r_{i-1} \\ (\mathbb{1} - M_{rc})r_i &= M_{ff}r_{i-1} \\ r_i &= (\mathbb{1} - M_{rc})^{-1}M_{ff}r_{i-1} \end{aligned} \quad (9)$$

331

332 Because inhibitory populations are assumed to have only recurrent projections, we can insert the expression  
 333 for each inhibitory population  $r_i^{I,j}$  into its respective  $r_i^{E,j}$  and reduce the system of equations to:

$$r_i^E = \kappa r_{i-1}^E \quad (10)$$

with  $r_i^E = (r_i^{E,0}, r_i^{E,1}, r_i^{E,2})^T$  and

$$\kappa = \begin{pmatrix} \frac{w_{ff}^{00}(kw_{rc}^0+1)}{kw_{rc}^0-w_{rc}^0+1} & \frac{-kw_{rc}^0w_{ffi}^{10}+kw_{rc}^0w_{ff}^{10}+w_{ff}^{10}}{kw_{rc}^0-w_{rc}^0+1} & \frac{-kw_{rc}^0w_{ffi}^{20}+kw_{rc}^0w_{ff}^{20}+w_{ff}^{20}}{kw_{rc}^0-w_{rc}^0+1} \\ \frac{-kw_{ffi}^{01}w_{rc}^1+kw_{ff}^{01}w_{rc}^1+w_{ff}^{01}}{kw_{rc}^1-w_{rc}^1+1} & \frac{w_{ff}^{11}(kw_{rc}^1+1)}{kw_{rc}^1-w_{rc}^1+1} & \frac{-kw_{rc}^1w_{ffi}^{21}+kw_{rc}^1w_{ff}^{21}+w_{ff}^{21}}{kw_{rc}^1-w_{rc}^1+1} \\ \frac{-kw_{ffi}^{02}w_{rc}^2+kw_{ff}^{02}w_{rc}^2+w_{ff}^{02}}{kw_{rc}^2-w_{rc}^2+1} & \frac{-kw_{ffi}^{12}w_{rc}^2+kw_{ff}^{12}w_{rc}^2+w_{ff}^{12}}{kw_{rc}^2-w_{rc}^2+1} & \frac{w_{ff}^{22}(kw_{rc}^2+1)}{kw_{rc}^2-w_{rc}^2+1} \end{pmatrix}$$

To connect parameters of the population based model to neurons, connection probabilities and synaptic strengths,

we proceed as in the non-linear rate model and set recurrent and feed-forward weights to

$$\begin{aligned} w_{rc}^j &= cM^{E,j}p_{rc}g_{rc} \\ w_{ff}^{jm} &= cM^{E,j}p_{ff}g_{ff}^{jm} \\ w_{ffi}^{jm} &= cM^{E,j}p_{ffi}g_{ffi}^{jm} \end{aligned} \quad (11)$$

334 with  $c$  a scaling parameter related to the slope of the neurons' input-output transfer function (Chenkov et al.,  
 335 2017, see below),  $M^{E,j}$  the number of neurons per excitatory assembly of sequence  $s^j$ ,  $p_{rc}$  and  $g_{rc}$ ,  $p_{ff}$  and  
 336  $g_{ff}^{jm}$ ,  $p_{ffi}$  and  $g_{ffi}^{jm}$ , the connection probabilities and synaptic weights for recurrent, feed-forward excitation and  
 337 feed-forward inhibition, respectively. Further, we assume that the network operates in an approximately balanced  
 338 state and set  $k = 1$ .

339 For the single sequence scenario, we can express the firing rate of  $r_i^{E,1}$  as a function of  $r_{i-1}^{E,1}$

$$r_i^{E,1} = \kappa_{1,1} r_{i-1}^{E,1} \quad (12)$$

Thus we can express the condition for marginally stable propagation of sequence  $s^1$  as

$$\kappa_{1,1} = M^{E,1}cg_{ff}^{11}p_{ff}^{11}(M^{E,1}cg_{rc}p_{rc} + 1) = 1 \quad (13)$$

340 We determine the minimal required recurrent connection probability by solving for  $p_{rc}$ .

$$p_{rc} = \frac{-M^{E,1}cg_{ff}^{11}p_{ff}^{11} + 1}{(M^{E,1})^2c^2g_{ff}^{11}g_{rc}p_{ff}^{11}} \quad (14)$$

341 Further, we also derive  $c$  from equation 13.

$$c = \frac{-g_{ff}^{11}p_{ff}^{11} + \sqrt{g_{ff}^{11}p_{ff}^{11}(g_{ff}^{11}p_{ff}^{11} + 4g_{rc}p_{rc})}}{2M^{E,1}g_{ff}^{11}g_{rc}p_{ff}^{11}p_{rc}} \quad (15)$$

342 We determine  $c = 0.163$  with the parameters of the successful example sequence  $s^2$  from Fig. 1c ( $p_{rc} =$   
 343  $0.035, p_{ff} = 0.01$ ) rounded to the third decimal. We keep  $c$  at this constant value throughout the article.

344 To study the relation between required feed-forward weight and excitatory population size in a competition  
 345 scenario, we add the influence of a competing sequence  $s^0$

$$r_i^{E,1} = \kappa_{1,1} r_{i-1}^{E,1} + \kappa_{0,1} r_{i-1}^{E,0} \quad (16)$$

Again we define the condition for marginal stability as

$$\kappa_{1,1} r_{i-1}^{E,1} + \kappa_{0,1} r_{i-1}^{E,0} = -M^{E,0} M^{E,1} c^2 g_{ff}^{01} g_{rc} p_{ff} p_{rc} r_{i-1}^{E,1} + M^{E,1} c g_{ff}^{11} p_{ff}^{11} (M^{E,1} c g_{rc} p_{rc} + 1) = 1 \quad (17)$$

and solve for  $p_{ff}^{11}$

$$p_{ff}^{11} = \frac{M^{E,0} r_{i-1}^{E,0} M^{E,1} c^2 g_{ff}^{01} g_{rc} p_{ff} p_{rc} + 1}{M^{E,1} c g_{ff}^{11} (M^{E,1} c g_{rc} p_{rc} + 1)} \quad (18)$$

<sup>346</sup> By setting  $r_{i-1}^{E,0}$  to 1 or 0, we can define a scenario with and without competition.

Table 1: Description of parameters in the non-linear rate model

Parameter	Description
$M^E,i$	number of excitatory neurons per assembly in $s^i$
$M^I,i$	number of inhibitory neurons per assembly inMemory replay in balanced recurrent networks $s^i$
$\tau$	population time constant [arbitrary units]
$a$	rightward shift of activation function
$g^E$	strength of excitatory synapses
$g^I$	strength of inhibitory synapses
$p_{rc}$	recurrent connection probability
$p_{ff}^{ii}$	feed-forward exc. connection probability between subsequent assemblies in $s^i$
$p_{ff}^{ij}$	feed-forward exc. connection probability between co-active assemblies in $s^i$ and $s^j$
$p_{ff,\Delta=1}^{ij}$	feed-forward exc. connection probability between subsequently active assemblies in $s^i$ and $s^j$
$p_{ffi}$	feed-forward inhibition connection probability
$n_{ass}$	number of assemblies per sequence
$r^0$	initial activity of first assembly
$t$	simulation time [arbitrary units]
$r_{min}$	minimal activity for classification
$r_{tol}$	activity tolerance for classification

Table 2: Parameters of the non-linear rate model For each figure and sequence. Ranges are indicated with (start, stop, stepsize). Dashed lines indicate values applying to multiple columns.

Parameter	Fig. 1		Fig. 2		Fig. 3		Fig. 4			Fig. 5		
	$s^0$	$s^0$	$s^1$	$s^0$	$s^1$	$s^0$	$s^1$	$s^2$	$s^0$	$s^1$	$s^2$	
$M^E$	800	(400, 2000, 100)		1000	(100, 2000, 100)	1000	500	500	1000	500	500	
$M^I$	200	(100, 500, 25)		250	(25, 500, 25)	250	125	125	250	125	125	
$\tau$	-----	-----	0.2	-----	-----	-----	-----	-----	-----	-----	-----	
$a$	-----	-----	-----	-----	-----	-----	$1 \times 10^{-7}$	-----	-----	-----	-----	
$g^E$	-----	-----	-----	-----	-----	-----	0.2	-----	-----	-----	-----	
$g^I$	-----	-----	-----	-----	-----	-----	0.7	-----	-----	-----	-----	
$p_{rc}$	(0.0, 0.1, 0.001)	(0.1, 0.05, 0.005)	-----	-----	-----	-----	0.05	-----	-----	-----	-----	
$p_{ff}^{ii}$	(0, 0.1, 0.001)	(0.01, 0.03, 0.002)	-----	(0.0, 0.1, 0.005)	-----	-----	0.02	-----	(0, 0.04, 0.001)	(0, 0.04, 0.001)	-----	
$p_{ff}^{ij}$	-----	-----	0	-----	-----	-----	(0, 0.04, 0.001)	(0, 0.04, 0.001)	(0, 0.04, 0.001)	(0, 0.04, 0.001)	-----	
$p_{ff,\Delta=1}^{ij}$	-----	-----	-----	0.	-----	-----	-----	-----	(0, 0.04, 0.001)	(0, 0.04, 0.001)	(0, 0.04, 0.001)	
$p_{ffi}$	0.01	(0.01, 0.01, 0.0005)	-----	-----	-----	-----	0.01	-----	-----	-----	-----	
$n_{ass}$	-----	-----	-----	-----	30	-----	-----	-----	-----	-----	-----	
$r^0$	-----	-----	-----	-----	0.5	-----	-----	-----	-----	-----	-----	
$t$	-----	-----	(0, 20, 0.02)	-----	-----	-----	-----	-----	(0, 50, 0.02)	(0, 50, 0.02)	-----	
$r_{min}$	-----	-----	-----	-----	0.01	-----	-----	-----	-----	-----	-----	
$r_{tol}$	-----	-----	-----	0.0001	-----	-----	-----	-----	-----	-----	-----	

## 347 References

- 348 Abeles, M., Hayon, G., and Lehmann, D. (2004). Modeling compositionality by dynamic binding of synfire  
349 chains. *Journal of Computational Neuroscience*, 17(2):179–201.
- 350 Amari, S.-i. (1977). Dynamics of pattern formation in lateral-inhibition type neural fields. *Biological cybernetics*,  
351 27(2):77–87.
- 352 Ambrose, R. E., Pfeiffer, B. E., and Foster, D. J. (2016). Reverse replay of hippocampal place cells is uniquely  
353 modulated by changing reward. *Neuron*, 91(5):1124–1136.
- 354 Arnoldi, H.-M. R. and Brauer, W. (1996). Synchronization without oscillatory neurons. *Biological Cybernetics*,  
355 74(3):209–223.
- 356 Azizi, A. H., Wiskott, L., and Cheng, S. (2013). A computational model for preplay in the hippocampus. *Frontiers*  
357 in computational neuroscience, 7:161.
- 358 Bragin, A., Jando, G., Nadasdy, Z., Van Landeghem, M., and Buzsáki, G. (1995). Dentate EEG spikes and asso-  
359 ciated interneuronal population bursts in the hippocampal hilar region of the rat. *Journal of Neurophysiology*,  
360 73(4):1691–1705.
- 361 Chenani, A., Sabariego, M., Schlesiger, M. I., Leutgeb, J. K., Leutgeb, S., and Leibold, C. (2019). Hippocampal  
362 CA1 replay becomes less prominent but more rigid without inputs from medial entorhinal cortex. *Nature*  
363 Communications, 10(1):1–13.
- 364 Chenzov, N., Sprekeler, H., and Kempter, R. (2017). Memory replay in balanced recurrent networks. *PLOS*  
365 *Computational Biology*, 13(1):e1005359.
- 366 Danjo, T., Toyoizumi, T., and Fujisawa, S. (2018). Spatial representations of self and other in the hippocampus.  
367 *Science*, 359(6372):213–218.
- 368 Diba, K. and Buzsáki, G. (2007). Forward and reverse hippocampal place-cell sequences during ripples. *Nature*  
369 *Neuroscience*, 10(10):1241.
- 370 Diesmann, M., Gewaltig, M.-O., and Aertsen, A. (1999). Stable propagation of synchronous spiking in cortical  
371 neural networks. *Nature*, 402(6761):529–533.
- 372 Dragoi, G. and Buzsáki, G. (2006). Temporal encoding of place sequences by hippocampal cell assemblies.  
373 *Neuron*, 50(1):145–157.
- 374 Dupret, D., O'Neill, J., Pleydell-Bouverie, B., and Csicsvari, J. (2010). The reorganization and reactivation of  
375 hippocampal maps predict spatial memory performance. *Nature Neuroscience*, 13(8):995–1002.

- 376 Eichenlaub, J.-B., Jarosiewicz, B., Saab, J., Franco, B., Kelemen, J., Halgren, E., Hochberg, L. R., and Cash,  
377 S. S. (2020). Replay of learned neural firing sequences during rest in human motor cortex. *Cell Reports*,  
378 31(5):107581.
- 379 Fernández-Ruiz, A., Oliva, A., de Oliveira, E. F., Rocha-Almeida, F., Tingley, D., and Buzsáki, G. (2019). Long-  
380 duration hippocampal sharp wave ripples improve memory. *Science*, 364(6445):1082–1086.
- 381 Fiete, I. R., Senn, W., Wang, C. Z., and Hahnloser, R. H. (2010). Spike-time-dependent plasticity and het-  
382 erosynaptic competition organize networks to produce long scale-free sequences of neural activity. *Neuron*,  
383 65(4):563–576.
- 384 Foster, D. J. and Wilson, M. A. (2006). Reverse replay of behavioural sequences in hippocampal place cells during  
385 the awake state. *Nature*, 440(7084):680.
- 386 Friedrich, R. W. and Laurent, G. (2001). Dynamic optimization of odor representations by slow temporal pattern-  
387 ing of mitral cell activity. *Science*, 291(5505):889–894.
- 388 Girardeau, G., Benchenane, K., Wiener, S. I., Buzsáki, G., and Zugaro, M. B. (2009). Selective suppression of  
389 hippocampal ripples impairs spatial memory. *Nature Neuroscience*, 12(10):1222.
- 390 Gupta, A. S., Van Der Meer, M. A. A., Touretzky, D. S., and Redish, A. D. (2010). Hippocampal replay is not a  
391 simple function of experience. *Neuron*, 65(5):695–705.
- 392 Hahnloser, R. H., Kozhevnikov, A. A., and Fee, M. S. (2002). An ultra-sparse code underlies the generation of  
393 neural sequences in a songbird. *Nature*, 419(6902):65–70.
- 394 He, H., Boehringer, R., Huang, A. J., Overton, E. T., Polygalov, D., Okanoya, K., and McHugh, T. J. (2020). CA2  
395 inhibition reduces the precision of hippocampal assembly reactivation. *bioRxiv*.
- 396 Hennequin, G., Vogels, T. P., and Gerstner, W. (2012). Non-normal amplification in random balanced neuronal  
397 networks. *Physical Review E*, 86(1):011909.
- 398 Hertz, J. (1997). Modelling synfire processing.
- 399 Igata, H., Ikegaya, Y., and Sasaki, T. (2021). Prioritized experience replays on a hippocampal predictive map for  
400 learning. *Proceedings of the National Academy of Sciences*, 118(1).
- 401 Itskov, V., Curto, C., Pastalkova, E., and Buzsáki, G. (2011). Cell assembly sequences arising from spike threshold  
402 adaptation keep track of time in the hippocampus. *Journal of Neuroscience*, 31(8):2828–2834.
- 403 Ji, D. and Wilson, M. A. (2007). Coordinated memory replay in the visual cortex and hippocampus during sleep.  
404 *Nature Neuroscience*, 10(1):100–107.

- 405 Kappel, D., Nessler, B., and Maass, W. (2014). STDP installs in winner-take-all circuits an online approximation  
406 to hidden Markov model learning. *PLOS Computational Biology*, 10(3).
- 407 Klos, C., Miner, D., and Triesch, J. (2018). Bridging structure and function: A model of sequence learning and  
408 prediction in primary visual cortex. *PLOS Computational Biology*, 14(6):e1006187.
- 409 Kumar, A., Rotter, S., and Aertsen, A. (2008). Conditions for propagating synchronous spiking and asynchronous  
410 firing rates in a cortical network model. *Journal of Neuroscience*, 28(20):5268–5280.
- 411 Kumar, A., Rotter, S., and Aertsen, A. (2010). Spiking activity propagation in neuronal networks: reconciling  
412 different perspectives on neural coding. *Nature Reviews Neuroscience*, 11(9):615.
- 413 Lee, H., Wang, C., Deshmukh, S. S., and Knierim, J. J. (2015). Neural population evidence of functional hetero-  
414 geneity along the CA3 transverse axis: pattern completion versus pattern separation. *Neuron*, 87(5):1093–1105.
- 415 Lehr, A. B., Kumar, A., and Tetzlaff, C. (2023). Sparse clustered inhibition projects sequential activity onto unique  
416 neural subspaces. *bioRxiv*, pages 2023–09.
- 417 Lehr, A. B., Kumar, A., Tetzlaff, C., Hafting, T., Fyhn, M., and Stöber, T. M. (2021). CA2 beyond social mem-  
418 ory: Evidence for a fundamental role in hippocampal information processing. *Neuroscience & Biobehavioral  
419 Reviews*, 126:398–412.
- 420 Lehr, A. B., Luboeinski, J., and Tetzlaff, C. (2022). Neuromodulator-dependent synaptic tagging and capture  
421 retroactively controls neural coding in spiking neural networks. *Scientific Reports*, 12(1):17772.
- 422 Lu, Y., Sato, Y., and Amari, S.-i. (2011). Traveling bumps and their collisions in a two-dimensional neural field.  
423 *Neural Computation*, 23(5):1248–1260.
- 424 Maes, A., Barahona, M., and Clopath, C. (2020a). Learning compositional sequences with multiple time scales  
425 through a hierarchical network of spiking neurons. *bioRxiv*.
- 426 Maes, A., Barahona, M., and Clopath, C. (2020b). Learning spatiotemporal signals using a recurrent spiking  
427 network that discretizes time. *PLOS Computational Biology*, 16(1):e1007606.
- 428 Mankin, E. A., Diehl, G. W., Sparks, F. T., Leutgeb, S., and Leutgeb, J. K. (2015). Hippocampal CA2 activity  
429 patterns change over time to a larger extent than between spatial contexts. *Neuron*, 85(1):190–201.
- 430 McNamara, C. G., Tejero-Cantero, Á., Trouche, S., Campo-Urriza, N., and Dupret, D. (2014). Dopaminergic  
431 neurons promote hippocampal reactivation and spatial memory persistence. *Nature Neuroscience*, 17(12):1658–  
432 1660.

- 433 Michaelis, C., Lehr, A. B., and Tetzlaff, C. (2020). Robust trajectory generation for robotic control on the neuro-  
434 morphic research chip loihi. *Frontiers in neurorobotics*, 14:589532.
- 435 Miner, D. and Tetzlaff, C. (2020). Hey, look over there: Distraction effects on rapid sequence recall. *Plos one*,  
436 15(4):e0223743.
- 437 Murphy, B. K. and Miller, K. D. (2009). Balanced amplification: a new mechanism of selective amplification of  
438 neural activity patterns. *Neuron*, 61(4):635–648.
- 439 Murray, J. M. et al. (2017). Learning multiple variable-speed sequences in striatum via cortical tutoring. *Elife*,  
440 6:e26084.
- 441 O'Keefe, J. (1976). Place units in the hippocampus of the freely moving rat. *Experimental Neurology*, 51(1):78–  
442 109.
- 443 Oliva, A., Fernández-Ruiz, A., Leroy, F., and Siegelbaum, S. A. (2020). Hippocampal CA2 sharp-wave ripples  
444 reactivate and promote social memory. *Nature*, 587(7833):264–269.
- 445 Omer, D. B., Maimon, S. R., Las, L., and Ulanovsky, N. (2018). Social place-cells in the bat hippocampus.  
446 *Science*, 359(6372):218–224.
- 447 Recanatesi, S., Katkov, M., Romani, S., and Tsodyks, M. (2015). Neural network model of memory retrieval.  
448 *Frontiers in computational neuroscience*, 9:149.
- 449 Salz, D. M., Tiganj, Z., Khasnabish, S., Kohley, A., Sheehan, D., Howard, M. W., and Eichenbaum, H. (2016).  
450 Time cells in hippocampal area CA3. *Journal of Neuroscience*, 36(28):7476–7484.
- 451 Seeholzer, A., Deger, M., and Gerstner, W. (2019). Stability of working memory in continuous attractor networks  
452 under the control of short-term plasticity. *PLoS computational biology*, 15(4):e1006928.
- 453 Silva, D., Feng, T., and Foster, D. J. (2015). Trajectory events across hippocampal place cells require previous  
454 experience. *Nature Neuroscience*, 18(12):1772.
- 455 Singer, A. C. and Frank, L. M. (2009). Rewarded outcomes enhance reactivation of experience in the hippocampus.  
456 *Neuron*, 64(6):910–921.
- 457 Skaggs, W. E. and McNaughton, B. L. (1996). Replay of neuronal firing sequences in rat hippocampus during  
458 sleep following spatial experience. *Science*, 271(5257):1870.
- 459 Spalla, D., Cornacchia, I. M., and Treves, A. (2021). Continuous attractors for dynamic memories. *Elife*,  
460 10:e69499.

- 461 Spreizer, S., Aertsen, A., and Kumar, A. (2019). From space to time: Spatial inhomogeneities lead to  
462 the emergence of spatiotemporal sequences in spiking neuronal networks. *PLOS Computational Biology*,  
463 15(10):e1007432.
- 464 Stöber, T. M., Lehr, A. B., Hafting, T., Kumar, A., and Fyhn, M. (2020). Selective neuromodulation and mutual  
465 inhibition within the CA3–CA2 system can prioritize sequences for replay. *Hippocampus*, 30(11):1228–1238.
- 466 Tetzlaff, C., Dasgupta, S., Kullvicius, T., and Wörgötter, F. (2015). The use of hebbian cell assemblies for nonlinear  
467 computation. *Scientific reports*, 5(1):12866.
- 468 Vogels, T. P., Sprekeler, H., Zenke, F., Clopath, C., and Gerstner, W. (2011). Inhibitory plasticity balances excita-  
469 tion and inhibition in sensory pathways and memory networks. *Science*, 334(6062):1569–1573.
- 470 Wilson, H. R. and Cowan, J. D. (1972). Excitatory and inhibitory interactions in localized populations of model  
471 neurons. *Biophysical Journal*, 12(1):1–24.
- 472 Wilson, M. A., McNaughton, B. L., et al. (1994). Reactivation of hippocampal ensemble memories during sleep.  
473 *Science*, 265(5172):676–679.
- 474 Wintzer, M. E., Boehringer, R., Polygalov, D., and McHugh, T. J. (2014). The hippocampal CA2 ensemble is  
475 sensitive to contextual change. *The Journal of Neuroscience*, 34(8):3056–3066.
- 476 Yamamoto, J. and Tonegawa, S. (2017). Direct medial entorhinal cortex input to hippocampal CA1 is crucial for  
477 extended quiet awake replay. *Neuron*, 96(1):217–227.
- 478 York, L. C. and van Rossum, M. C. (2009). Recurrent networks with short term synaptic depression. *Journal of  
479 computational neuroscience*, 27(3):607–620.